

Improving prediction accuracy of spread through air spaces in clinical-stage T1N0 lung adenocarcinoma using computed tomography imaging models



Shihua Dou, MD,^{a,b,c} Zhuofeng Li, BS,^d Zhenbin Qiu, MD,^{e,f,g} Jing Zhang, PhD,^d Yaxi Chen, MD,^{a,b} Shuyuan You, MD,^b Mengmin Wang, MD,^{f,g} Hongsheng Xie, MD,^{a,b} Xiaoxiang Huang, MD,^{a,b} Yun Yi Li,^e Jingjing Liu, MD,^{a,b} Yuxin Wen, MD,^b Jingshan Gong, PhD,^b Fanli Peng, MD,^b Wenzhao Zhong, PhD,^{e,f,g} Xuegong Zhang, PhD,^{d,h} and Lin Yang, PhD^{a,b}

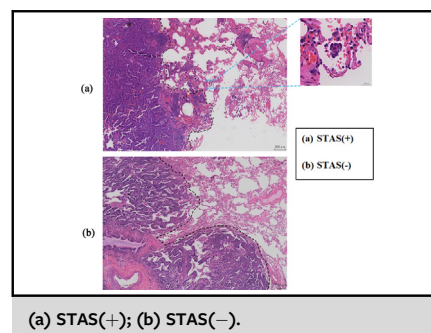
ABSTRACT

Objectives: To develop computed tomography (CT)-based models to increase the prediction accuracy of spread through air spaces (STAS) in clinical-stage T1No lung adenocarcinoma.

Methods: Three cohorts of patients with stage T1No lung adenocarcinoma ($n = 1258$) were analyzed retrospectively. Two models using radiomics and deep neural networks (DNNs) were established to predict the lung adenocarcinoma STAS status. For the radiomic models, features were extracted using PyRadiomics, and 10 features with nonzero coefficients were selected using least absolute shrinkage and selection operator regression to construct the models. For the DNN models, a 2-stage (supervised contrastive learning and fine-tuning) deep-learning model, MultiCL, was constructed using CT images and the STAS status as training data. The area under the curve (AUC) was used to verify the predictive ability of both model types for the STAS status.

Results: Among the radiomic models, the linear discriminant analysis model exhibited the best performance, with AUC values of 0.8944 (95% confidence interval [CI], 0.8241-0.9502) and 0.7796 (95% CI, 0.7089-0.8448) for predicting the STAS status on the test and external validation cohorts, respectively. Among the DNN models, MultiCL exhibited the best performance, with AUC values of 0.8434 (95% CI, 0.7580-0.9154) for the test cohort and 0.7686 (95% CI, 0.6991-0.8316) for the external validation cohort.

Conclusions: CT-based imaging models (radiomics and DNNs) can accurately identify the STAS status of clinical-stage T1No lung adenocarcinoma, potentially guiding surgical decision making and improving patient outcomes. (JTCVS Open 2024;21:290-303)



(a) STAS(+); (b) STAS(-).

CENTRAL MESSAGE

CT imaging models accurately predict STAS status in clinical-stage T1No lung adenocarcinoma, aid decision making regarding the extent of anatomic lung resection, and improve patient outcomes.

PERSPECTIVE

Current surgical approaches for clinical-stage T1No lung adenocarcinoma with STAS require refinement because of the worse prognosis associated with sublobectomy compared to lobectomy. Our CT-based radiomic and DNN models improve prediction accuracy, guiding the surgical extent and advancing personalized treatment strategies.

From the ^aSecond Clinical Medical College, Jinan University, Shenzhen, China; ^bShenzhen People's Hospital, Second Clinical Medical College, Jinan University, First Affiliated Hospital of South University of Science and Technology of China, Shenzhen Institute of Respiratory Diseases, Shenzhen, China; ^cDepartment of Thoracic Surgery, First Affiliated Hospital of Hainan Medical University, Hainan Province Clinical Medical Center of Respiratory Disease, Haikou, China; ^dBioinformatics Division, Department of Automation, BNRIST and MOE Key Lab of Bioinformatics, Tsinghua University, Beijing, China; ^eSchool of Medicine, South China University of Technology, Guangzhou, China; ^fGuangdong Lung Cancer Institute, Guangdong Provincial People's Hospital (Guangdong Academy of Medical Sciences), Southern Medical University, Guangzhou, China; ^gGuangdong


Provincial Key Laboratory of Translational Medicine in Lung Cancer, Guangdong Provincial People's Hospital (Guangdong Academy of Medical Sciences), Southern Medical University, Guangzhou, China; and ^hSchool of Medicine, Tsinghua University, Beijing, China.

This work was partially supported by the National Science Foundation of China (Grant 82241235), the National Key R&D Program of China (2021YFF1200901), the High-level Hospital Construction Project (DFJH201801), the Guangdong Basic and Applied Basic Research Foundation (2019B1515130002), and the Guangdong Provincial Key Laboratory of Lung Cancer Translational Medicine (2017B030314120).

Shihua Dou, Zhuofeng Li, and Zhenbin Qiu contributed equally to this work.

Abbreviations and Acronyms

| | |
|------|--|
| 3D | = 3-dimensional |
| AUC | = area under the curve |
| CI | = confidence interval |
| CT | = computed tomography |
| DNN | = deep neural network |
| GDPH | = Guangdong Provincial People's Hospital |
| JCOG | = Japan Clinical Oncology Group |
| LDA | = linear discriminant analysis |
| OR | = odds ratio |
| OS | = overall survival |
| RFS | = recurrence-free survival |
| STAS | = spread through air spaces |
| SZPH | = Shenzhen People's Hospital |

 Supplemental material is available online.

Among the diverse histologic manifestations of lung cancer, lung adenocarcinoma stands out as the most frequently occurring subtype. Surgical excision is considered the gold standard treatment for early-stage lung cancer (T1N0M0, ninth edition tumor-node-metastasis stage) and boasts a 5-year survival rate exceeding 80%.¹ However, studies have indicated that 13% to 23% of patients relapse after surgery,^{2,3} which could be attributed to the distinctive invasion pattern of the tumor.

In 2015, the World Health Organization formally introduced spread through air spaces (STAS) as a novel lung adenocarcinoma invasion mechanism.⁴ STAS refers to micropapillary clusters, solid nests, or single cells extending past the tumor margin into the air spaces of the surrounding lung parenchyma. Recent studies suggest that the presence of STAS correlates with an unfavorable prognosis in early-stage lung cancer, especially for patients in stage I; however, its prognostic value appears to be less significant for patients in stages II and III.^{5,6}

According to results from the Japan Clinical Oncology Group (JCOG 0804),⁷ JCOG 0802,⁸ JCOG 1211,⁹ and Cancer and Leukemia Group B 140503,¹⁰ an increasing number of patients with early lung cancer involving tumors 1 to 3 cm in size (clinical stage T1N0) will undergo sublobectomy. However, research suggests that patients with

STAS-positive status experience a notably reduced recurrence-free survival (RFS) rate when undergoing sublobectomy compared to lobectomy.¹¹⁻¹⁴ In clinical-stage T1N0 lung adenocarcinoma, the STAS positivity rate ranges from 11.6% to 39.5%.^{12,15-19} Preoperative or intraoperative identification of STAS can optimize the surgical modality and improve the prognosis for affected patients. Although intraoperative frozen section detection of STAS has limitations owing to its low sensitivity,²⁰ the pathologic diagnosis of STAS remains vital. At present, STAS detection still relies on a postoperative paraffin biopsy; therefore, noninvasive preoperative STAS identification can facilitate the correct selection of patients eligible for sublobectomy.

Computed tomography (CT) is a valuable noninvasive diagnostic tool for various cancers, including lung adenocarcinoma, enabling accurate diagnosis, staging, and monitoring. CT imaging offers detailed visualizations of tumor tissue, capturing morphologic and textural details,²¹ including many computational features not perceived by the human eye.²² This suggests the possibility of preoperative identification of stage IA adenocarcinoma STAS from a radiomic perspective.^{23,24} Two primary STAS recognition methods using CT images are currently available, one based on the construction of a radiomic model for STAS identification²⁵⁻²⁸ and the other involving the use of a 3D convolutional neural network model.²⁹ In addition to CT models, nomograms³⁰ based on clinical characteristics and radiologic features have been used for STAS prediction; however, these models lack effective STAS status identification in clinical-stage T1N0 lung adenocarcinoma, external validation efficacy, and the prospect of widespread clinical use. Accordingly, an accurate, noninvasive, and easy-to-use preoperative STAS recognition model is needed.

The objective of the present study was to develop novel approaches using CT image-based models (radiomics and deep neural networks [DNNs]) for increasing the predictive accuracy of clinical-stage T1N0 lung adenocarcinoma STAS status. The noninvasiveness and discovery of imaging features invisible to the human eye are advantages of both methods, contributing to better preoperative STAS status identification.

MATERIALS AND METHODS**Patient Selection**

In compliance with the Declaration of Helsinki and applicable local laws, this study was approved by the Scientific Research Ethics

Dongmen North Rd, Luohu District, Shenzhen, China (E-mail: 13798314779@163.com)

2666-2736

Copyright © 2024 The Author(s). Published by Elsevier Inc. on behalf of The American Association for Thoracic Surgery. This is an open access article under the CC BY-NC-ND license (<http://creativecommons.org/licenses/by-nc-nd/4.0/>).
<https://doi.org/10.1016/j.xjcn.2024.07.018>

Received for publication March 4, 2024; revisions received July 17, 2024; accepted for publication July 22, 2024; available ahead of print Aug 15, 2024.

Address for reprints: Wenzhao Zhong, PhD, Guangdong Lung Cancer Institute, Guangdong Provincial People's Hospital, No. 106, Zhongshan 2nd Rd, Yuexiu District, Guangzhou 510080, China (E-mail: syzhongwenzhao@scut.edu.cn); or Xuegong Zhang, PhD, Bioinformatics Division, Tsinghua University, Haidian District, Beijing 100084, China (E-mail: zhangxg@tsinghua.edu.cn); or Lin Yang, PhD, Second Clinical Medical College of Shenzhen University, No. 1017,

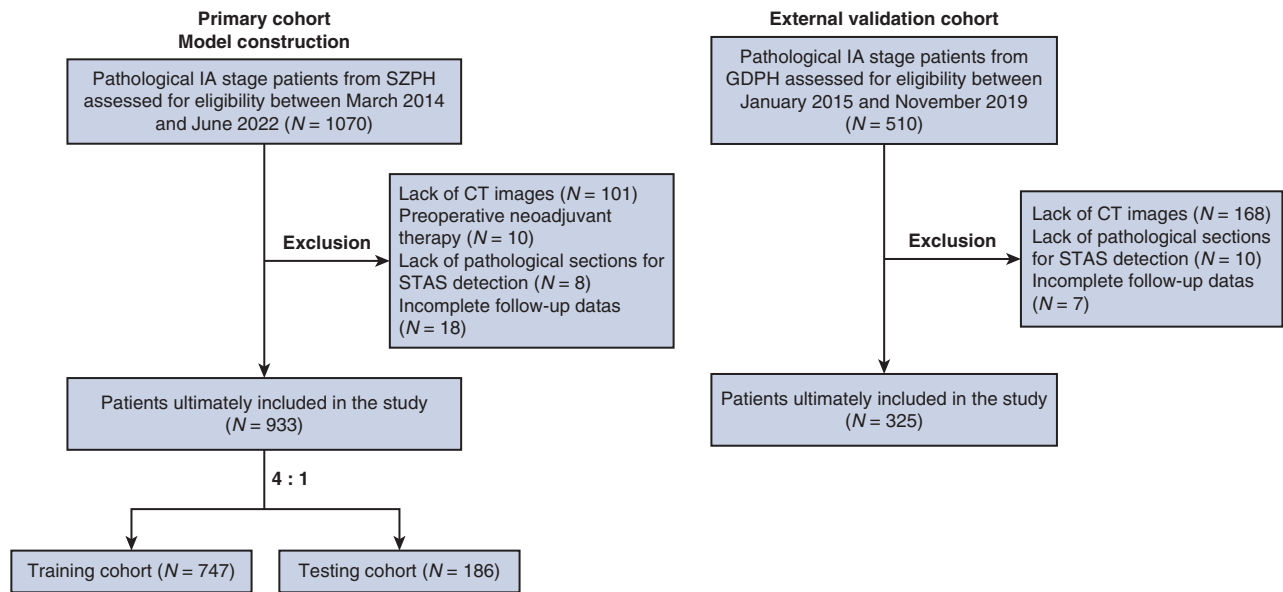


FIGURE 1. Recruitment flowchart for owed in this study.

Committees of both Shenzhen People's Hospital (SZPH) (LL-KY-2021916-01) and Guangdong Provincial People's Hospital (GDPH) (GDRHEC2019726H). Additionally, informed consent was secured from exempted subjects from the Ethics Committee. Only nonidentifiable information was used in this study.

The primary cohort comprised 933 patients who underwent curative surgical procedures at SZPH between March 2014 and June 2022. An independent validation cohort of 325 patients treated at GDPH between January 2015 and November 2019 was identified. Figure 1 illustrates the recruitment process for this study. Inclusion criteria were (1) existence of postoperative pathology indicating a primary lung malignancy, (2) postoperative pathologic diagnosis of lung adenocarcinoma, (3) postoperative pathological T stage of pT1 ($P \leq 3$ cm), and (4) age >18 years. Exclusion criteria included (1) postoperative pathology, including lymph node metastasis and metastasis from other sites; (2) incomplete clinical pathologic data or follow-up; (3) preoperative neoadjuvant therapy or postoperative adjuvant therapy; (4) history of other malignant tumors within 5 years; and (5) no tumor slices available for review.

Histopathologic Evaluation and Clinical Characteristics

After surgical resection, all specimens were embedded in paraffin, fully fixed with a 4% formaldehyde solution, and then processed into conventional pathologic staining sections through dehydration, embedding, sectioning, and staining. Two pathologists (Drs You and Peng) reviewed all tumor biopsies. In cases of disagreement, a third pathologist (Dr Wen) was consulted. All pathologists had >3 years of expertise. Their assessments adhered to the STAS definition of the World Health Organization to determine a consensus STAS status; additional details are provided in the Online Data Supplement. Representative histopathologic samples illustrating STAS (+) and STAS (−) nodules are presented in Figure 2.

Patient medical records were reviewed to gather clinical characteristics, including age, sex, smoking status, pathologic staging, location, tumor size, histologic type, lung adenocarcinoma grade, micropapillary/solid $\geq 1\%$, surgical method, STAS status, and recurrence/metastasis. The lung adenocarcinoma grade³¹ is classified as follows: grade 1, lepidic predominant tumor; grade 2, acinar or papillary predominant tumor, both with no or $<20\%$ high-grade patterns; or grade 3, any tumor with $\geq 20\%$ high-grade pattern (solid, micropapillary, or complex gland).

CT Acquisition and Segmentation

The CT image acquisition process and the intraobserver (reader1 twice) and interobserver (reader1 vs reader2) reproducibility evaluations are described in the Online Data Supplement.

Data Preprocessing and Splitting

The thoracic CT images were reconstructed into a $512 \times 512 \times N$ matrix, with N denoting the total number of image slices. This reconstruction strategy resulted in variable pixel spacing and slice thickness among patients. B-spline interpolation was applied to standardize the spacing along

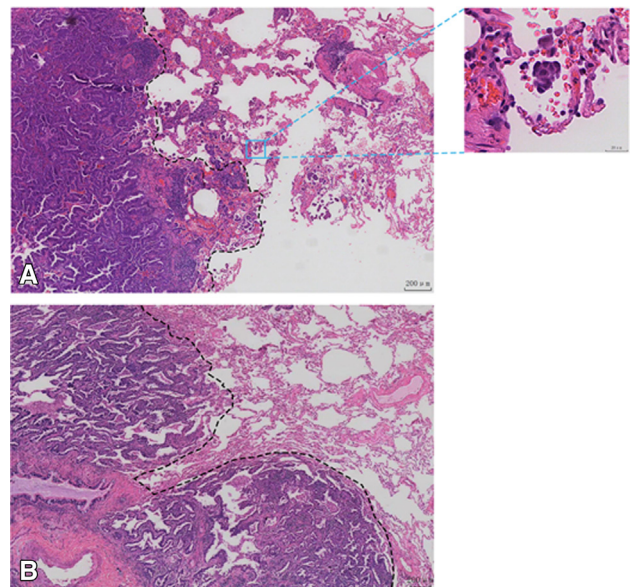


FIGURE 2. Definition of STAS-positive in histologic examination: STAS-positive was defined as the presence of tumor cells in the lung space beyond the margin of the primary tumor ($\times 10$ objective lens, $\times 10$ magnification). A, STAS-positive case (blue box, $\times 80$ magnification) and B, STAS-negative.

the 3 dimensions, resulting in a fixed resolution of $1 \times 1 \times 1 \text{ mm}^3$. This approach mitigates the effects of differing scales on the classification performance. Multiple 3D nodule image blocks of different sizes were sampled around the tumor center, including $16 \times 16 \times 16$, $32 \times 32 \times 32$, and $48 \times 48 \times 48 \text{ mm}^3$, to extract both the local features of the tumor and the global features of its surrounding area. All images were uniformly resized to a fixed size of $32 \times 32 \times 32$ voxels and served as the neural network input.

The primary cohort was randomly partitioned into training and testing cohorts at a 4:1 ratio, ensuring a consistent proportion of STAS-negative and STAS-positive patients across both cohorts. The external validation cohort consisted of an independent cohort of 325 patients sourced from GDPH.

STAS Status Prediction with Radiomics and DNNs

The comprehensive structure for building the radiomic model, as illustrated in Figure 3, A, encompassed feature extraction, feature selection, model training, and model evaluation. In addition to radiomics, we propose a 2-stage training strategy, MultiCL, which includes a supervised contrastive learning stage and a fine-tuning stage. The general scheme for these 2 stages is depicted in Figure 3, B. The STAS prediction process using the radiomic and DNN models is presented in the Online Data Supplement.

Statistical Analysis

Statistical analyses were conducted using R version 3.6.3 (R Foundation for Statistical Computing) and Python version 3.7 (<https://www.python.org/>). Continuous variables are expressed as mean \pm standard deviation and range, and qualitative variables are expressed as raw number, proportion, and percentage. The Kolmogorov-Smirnov test was used to assess the normality of the continuous variables. If the variable followed a normal distribution, the *t* test was used; otherwise, the Mann-Whitney *U* test was used. The χ^2 test was applied to the qualitative variables. The receiver operating characteristic curve and area under the curve (AUC) were computed to assess the model performance.

The RFS and overall survival (OS) curves were derived from all available follow-up data utilizing Kaplan-Meier estimates. These curves were subsequently compared using a log-rank test. Logistic regression analysis was conducted for both univariate and multivariate analyses. The follow-up data and endpoints are presented in the Online Data Supplement.

RESULTS

Patient Baseline Characteristics

This study included 933 patients with pathologically confirmed stage T1N0 lung adenocarcinoma at SZPH. Among them, 838 patients had no STAS and 95 had STAS. The basic clinical data for the training and testing cohorts are presented in Table 1. Notably, the testing cohort and training cohort exhibited comparable baseline characteristics.

The basic clinical characteristics of stage T1N0 lung adenocarcinoma regarding STAS status are presented in Table 2. According to the Kaplan-Meier method and log-rank test in the survival analysis, the RFS rate was 98.7% and the OS rate was 99.7% for the entire primary cohort. The 5-year RFS rate was statistically significantly higher for the STAS-negative group compared to the STAS-positive group (97.2% vs 91.4%; $P < .001$). Similarly, the 5-year OS rate was statistically significantly higher in the STAS-negative group (100% vs 94.7%; $P < .001$). In the

validation cohort, the RFS rate was 96.0% and the OS rate was 97.8%. Analogously, the 5-year RFS rate was statistically significantly higher for the STAS-negative group compared to the STAS-positive group (98.1% vs 84.8%; $P < .001$), as was the 5-year OS rate (99.3% vs 88.7%; $P < .001$). The survival analysis results are shown in Figure 4.

The results of the univariate analyses based on logistic regression show that sex, age, smoking status, tumor size, lung adenocarcinoma grade, and micropapillary/solid $\geq 1\%$ were significantly correlated with the STAS-positive condition ($P < .01$). On multivariate analysis, tumor size, lung adenocarcinoma grade, and micropapillary/solid $\geq 1\%$ were correlated with the STAS-positive condition ($P < .01$). The results of the univariate and multivariate analyses are presented in Online Data Supplement.

Predictive Performance of Radiomic Models for STAS Status

The diagnostic efficiencies of the 9 machine learning models are presented in Online Data Supplement. The AUCs for the training, testing, and external validation cohorts were calculated, as shown in Figure 5, A. The AdaBoost model achieved the highest diagnostic efficiency in the training cohort, with an AUC of 0.9678 (95% CI, 0.9466-0.9848). The linear discriminant analysis (LDA) model achieved the highest diagnostic efficiency among the 9 machine learning models in the testing and external validation cohorts. The AUC values of the LDA model for the testing and external validation cohorts were 0.8944 (95% CI, 0.8241-0.9502) and 0.7796 (95% CI, 0.7089-0.8448), respectively.

Predictive Performance of DNN-Based Models for STAS Status

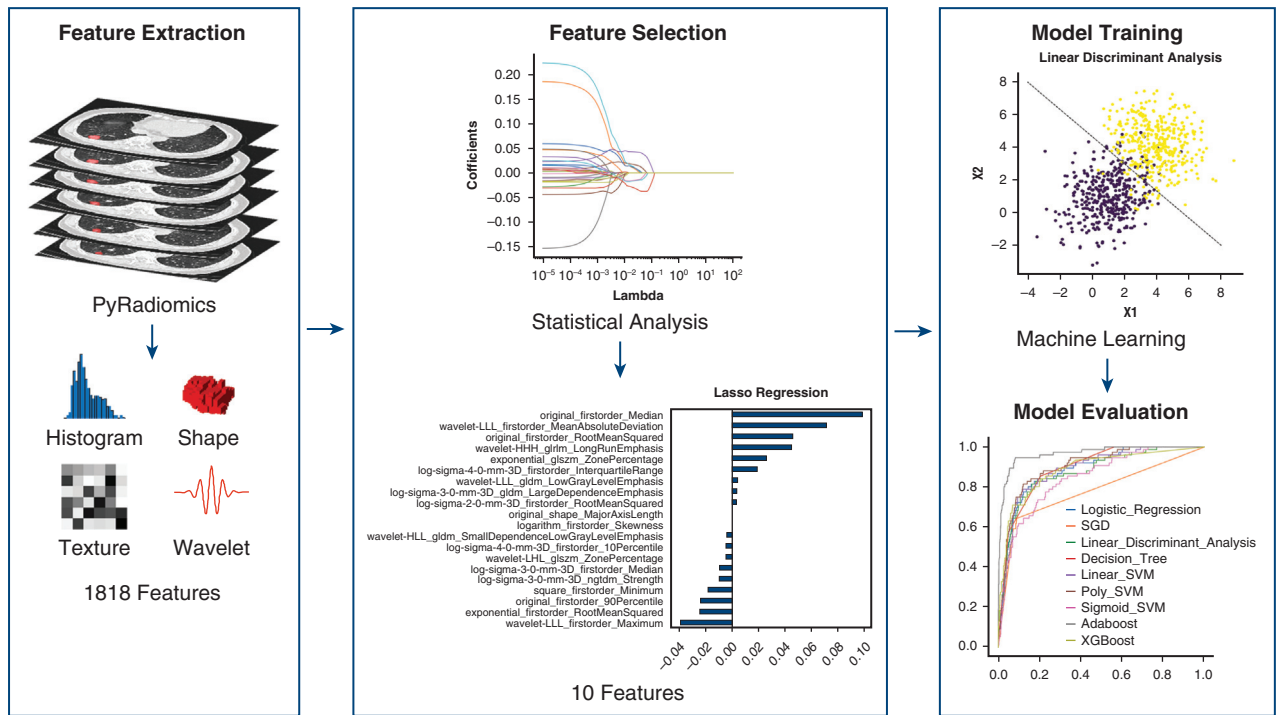
The diagnostic efficiencies of the DNN-based models are presented in Online Data Supplement. The MultiCL model achieved the highest diagnostic efficiency, with AUC values of 0.9995 (95% CI, 0.9986-1.0000) for the training cohort, 0.8434 (95% CI, 0.7580-0.9154) for the testing cohort, and 0.7686 (95% CI, 0.6991-0.8316) for the external validation cohort, as shown in Figure 5, B.

Clinical Application

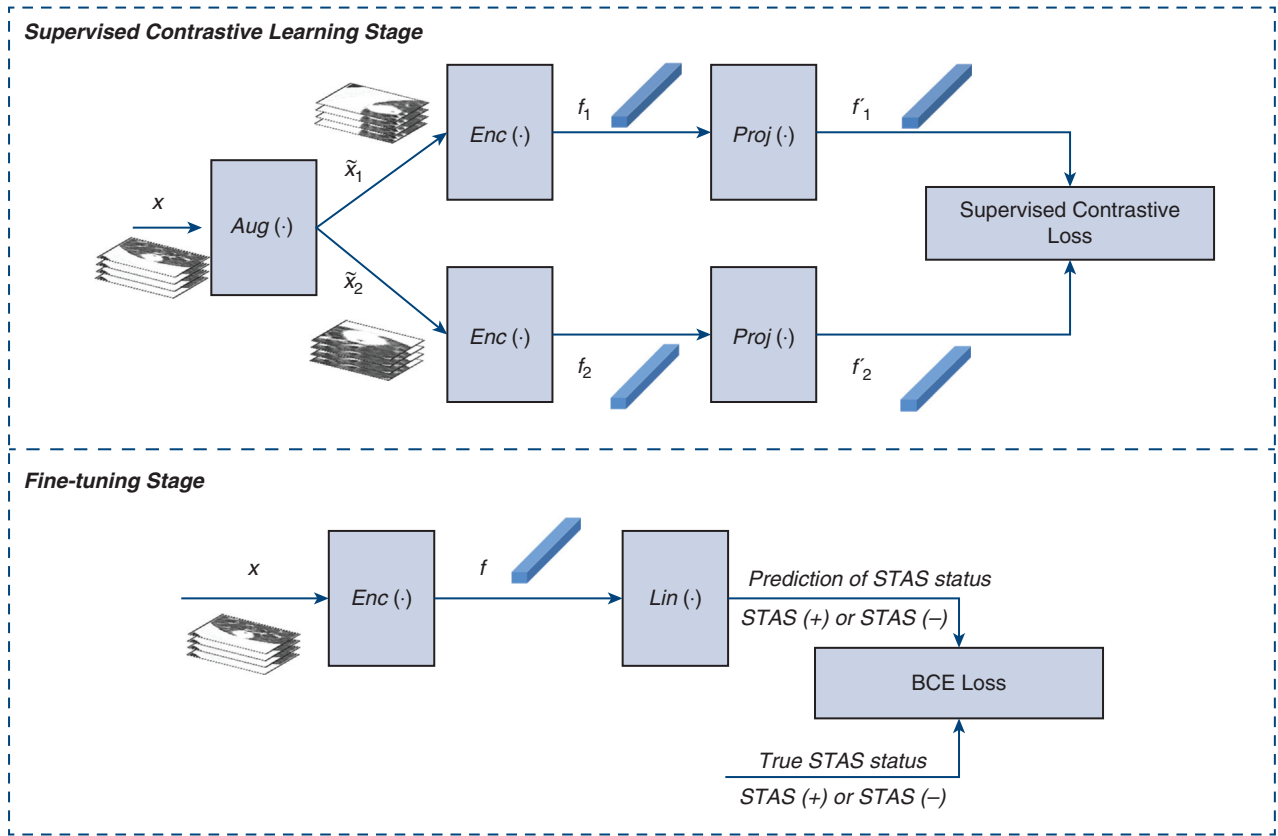
The results of decision curve analysis conducted for the LDA and MultiCL models (Online Data Supplement) indicate that when the threshold probability exceeded 5%, the MultiCL model was advantageous for STAS prediction compared to treating all or none of the patients within certain risk threshold ranges.

DISCUSSION

In this study, we developed novel approaches using 2 machine learning models—radiomics and DNNs—for



A



B

FIGURE 3. A, Overall framework for constructing the radiomic model. B, Overall MultiCL model framework. Single-channel 3D images are used as an example. In the actual training process, multi-channel 3D images are used as the deep neural network input.

TABLE 1. Basic clinical characteristics of the training and testing cohorts

| Characteristic | All patients (N = 933) | Training cohort (N = 747) | Testing cohort (N = 186) | P value |
|----------------------------------|------------------------|---------------------------|--------------------------|---------|
| Age, y, mean ± SD | 53.14 ± 13.00 | 53.02 ± 12.93 | 53.60 ± 13.23 | .589 |
| Sex, n (%) | | | | |
| Male | 359 (38.48) | 290 (38.82) | 69 (37.10) | .665 |
| Female | 574 (61.52) | 457 (61.18) | 117 (62.90) | |
| Smoking status, n (%) | | | | |
| Yes | 133 (14.26) | 106 (14.19) | 27 (14.52) | .909 |
| No | 800 (85.75) | 641 (85.81) | 159 (85.49) | |
| Pathological staging, n (%)* | | | | |
| Tis | 107 (11.47) | 20 (10.75) | 87 (11.64) | .707 |
| T1mi | 157 (16.83) | 36 (19.35) | 121 (16.20) | |
| T1a | 300 (32.15) | 53 (28.50) | 247 (33.07) | |
| T1b | 307 (32.91) | 64 (34.41) | 243 (32.53) | |
| T1c | 62 (6.64) | 13 (6.99) | 49 (6.56) | |
| Location, n (%) | | | | |
| LUL | 244 (26.15) | 201 (26.91) | 43 (23.12) | .339 |
| LLL | 132 (14.15) | 105 (14.06) | 27 (14.52) | |
| RUL | 320 (34.29) | 250 (33.47) | 70 (37.63) | |
| RML | 73 (7.82) | 54 (7.23) | 19 (10.22) | |
| RLL | 164 (17.58) | 137 (18.34) | 27 (14.52) | |
| Tumor size, n (%) | | | | |
| ≤1 cm | 548 (58.74) | 443 (59.30) | 105 (56.45) | .779 |
| 1-2 cm | 323 (34.62) | 255 (34.14) | 68 (36.56) | |
| >2-3 cm | 62 (6.65) | 49 (6.56) | 13 (6.99) | |
| Histologic type, n (%) | | | | .007 |
| AIS | 107 (11.47) | 87 (11.65) | 20 (10.75) | |
| IAC | 521 (55.84) | 423 (56.63) | 98 (52.69) | |
| MIA | 300 (32.16) | 236 (31.59) | 64 (34.41) | |
| MPA | 5 (0.53) | 1 (0.13) | 4 (2.15) | |
| Lung adenocarcinoma grade, n (%) | | | | |
| 1 | 468 (50.16) | 375 (50.20) | 93 (50.00) | .427 |
| 2 | 434 (46.52) | 350 (46.85) | 84 (45.16) | |
| 3 | 31 (3.32) | 22 (2.95) | 9 (4.84) | |
| Micropapillary/solid ≥1%, n (%) | | | | |
| Yes | 70 (7.50) | 56 (7.50) | 14 (7.53) | .989 |
| No | 863 (92.50) | 691 (92.50) | 172 (92.47) | |
| Surgical method, n (%) | | | | |
| Lobectomy | 420 (45.02) | 332 (44.44) | 88 (47.31) | .482 |
| Sublobectomy | 513 (54.98) | 415 (55.56) | 98 (52.69) | |
| STAS, n (%) | | | | |
| Positive | 95 (10.18) | 76 (10.17) | 19 (10.22) | .987 |
| Negative | 838 (89.82) | 671 (89.83) | 167 (89.79) | |
| Recurrence/metastasis, n (%) | | | | |
| Yes | 12 (1.29) | 10 (1.34) | 2 (1.08) | .775 |
| No | 921 (98.71) | 737 (98.66) | 184 (98.93) | |
| Death, n (%) | | | | |
| Yes | 3 (0.32) | 2 (0.27) | 1 (0.54) | .561 |
| No | 930 (99.68) | 745 (99.73) | 185 (99.46) | |

LUL, Left upper lobe; LLL, left lower lobe; RUL, right upper lobe; RML, right middle lobe; RLL, right lower lobe; AIS, adenocarcinoma in situ; IAC, invasive adenocarcinoma; MIA, minimally invasive adenocarcinoma; MPA, mucin-producing adenocarcinoma of the lung. *As assessed using the ninth edition of the tumor-node-metastasis staging system.

TABLE 2. Characteristics of patients in the primary and validation cohorts

| Characteristic | Primary cohort | | | Validation cohort | | |
|----------------------------------|----------------------------|---------------------------|---------|----------------------------|---------------------------|---------|
| | STAS-negative (N = 838) | STAS-positive (N = 95) | P value | STAS-negative (N = 266) | STAS-positive (N = 59) | P value |
| Age, y, mean ± SD | 52.42 ± 13.10 | 59.45 ± 10.06 | <.001 | 58.59 ± 11.61 | 61.53 ± 10.24 | .075 |
| Sex, n (%) | | | | | | |
| Male | 304 (36.28) | 55 (57.90) | <.001 | 97 (36.47) | 37 (62.71) | <.001 |
| Female | 534 (63.72) | 40 (42.11) | | 169 (63.53) | 22 (37.29) | |
| Smoking status, n (%) | | | | | | |
| Yes | 108 (12.89) | 25 (26.32) | <.001 | 41 (15.41) | 22 (37.29) | <.001 |
| No | 730 (87.11) | 70 (73.68) | | 225 (84.59) | 37 (62.71) | |
| Pathological staging, n (%)* | | | | | | |
| Tis | 107 (12.77) | 0 (0.00) | | 0 (0.00) | 0 (0.00) | |
| T1mi | 300 (35.80) | 0 (0.00) | | 0 (0.00) | 0 (0.00) | |
| T1a | 158 (18.85) | 13 (13.68) | | 34 (12.78) | 1 (1.70) | |
| T1b | 234 (27.92) | 59 (62.11) | | 151 (56.77) | 28 (47.46) | |
| T1c | 39 (4.65) | 23 (24.21) | | 81 (30.45) | 30 (50.85) | |
| Location, n (%) | | | | | | |
| LUL | 222 (26.49) | 22 (23.16) | .076 | 64 (24.06) | 15 (25.42) | .45 |
| LLL | 114 (13.60) | 18 (18.95) | | 35 (13.16) | 10 (16.95) | |
| RUL | 293 (34.96) | 27 (28.42) | | 101 (37.97) | 17 (28.81) | |
| RML | 69 (8.23) | 4 (4.21) | | 22 (8.27) | 3 (5.09) | |
| RLL | 140 (16.71) | 24 (25.26) | | 44 (16.54) | 14 (23.73) | |
| Tumor size, n (%) | | | | | | |
| ≤1 cm | 535 (63.84) | 13 (13.68) | <.001 | 34 (12.78) | 1 (1.70) | .002 |
| 1-2 cm | 264 (31.50) | 59 (62.11) | | 151 (56.77) | 28 (47.46) | |
| >2-3 cm | 39 (4.65) | 23 (24.21) | | 81 (30.45) | 30 (50.85) | |
| Histologic type, n (%) | | | | | | |
| AIS | 107 (12.77) | 0 (0.00) | | 0 (0.00) | 0 (0.00) | |
| IAC | 430 (51.31) | 91 (95.79) | | 266 (100.00) | 59 (100.00) | |
| MIA | 300 (35.80) | 0 (0.00) | | 0 (0.00) | 0 (0.00) | |
| MPA | 1 (0.12) | 4 (4.21) | | 0 (0.00) | 0 (0.00) | |
| Lung adenocarcinoma grade, n (%) | | | | | | |
| 1 | 465 (55.49) | 3 (3.16) | <.001 | 64 (24.06) | 3 (5.09) | <.001 |
| 2 | 365 (43.56) | 69 (72.63) | | 197 (74.06) | 46 (77.97) | |
| 3 | 8 (0.96) | 23 (24.21) | | 5 (1.88) | 10 (16.95) | |
| Micropapillary/solid ≥1%, n (%) | | | | | | |
| Yes | 15 (1.79) | 55 (57.10) | <.001 | 13 (4.89) | 21 (35.59) | <.001 |
| No | 823 (98.21) | 40 (42.11) | | 253 (95.11) | 38 (64.41) | |
| Surgical method, n (%) | | | | | | |
| Lobectomy | 359 (42.84) | 61 (64.21) | <.001 | 141 (53.01) | 45 (76.27) | .001 |
| Sublobectomy | 479 (57.16) | 34 (35.79) | | 125 (46.99) | 14 (23.73) | |
| Recurrence/metastasis, n (%) | | | | | | |
| Yes | 6 (0.72) | 6 (6.32) | <.001 | 4 (1.50) | 9 (15.25) | <.001 |
| No | 832 (99.28) | 89 (93.68) | | 262 (98.50) | 50 (84.75) | |
| Death, n (%) | | | | | | |
| Yes | 0 (0.00) | 3 (3.16) | | 1 (0.38) | 6 (10.17) | <.001 |
| No | 838 (100.00) | 92 (96.84) | | 265 (99.62) | 53 (89.83) | |

LUL, Left upper lobe; LLL, left lower lobe; RUL, right upper lobe; RML, right middle lobe; RLL, right lower lobe; AIS, adenocarcinoma in situ; IAC, invasive adenocarcinoma; MIA, minimally invasive adenocarcinoma; MPA, mucin-producing adenocarcinoma of the lung. *Assessed using the ninth edition of the tumor-node-metastasis staging system.

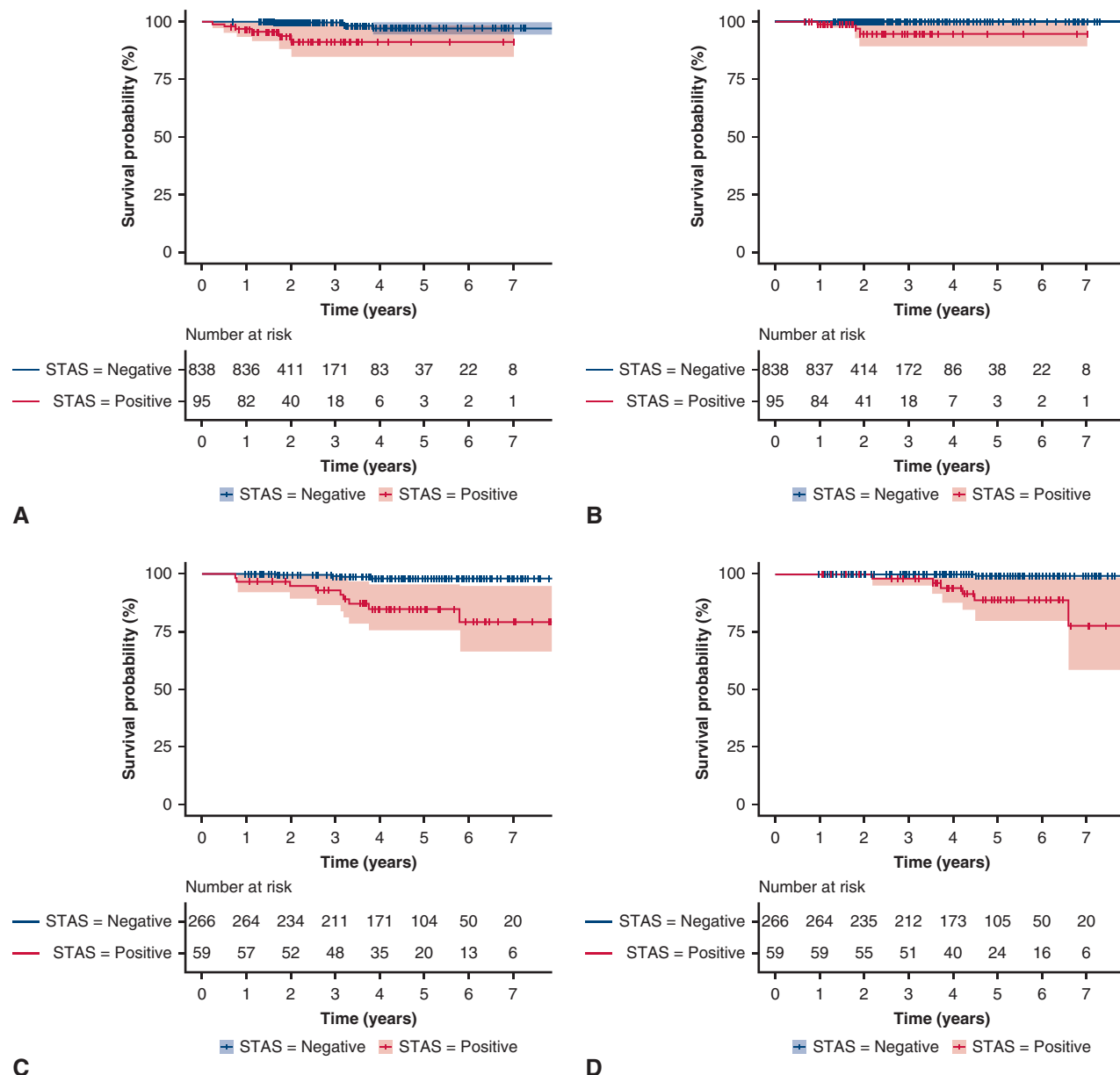


FIGURE 4. Kaplan-Meier curves (with 95% confidence interval) of relapse-free survival (RFS) and overall survival (OS). According to the Kaplan-Meier method and log-rank test in the survival analysis, for all patients in the primary cohort, the RFS rate was 98.7% and the OS rate was 99.7%. A, The 5-year RFS rate was statistically significantly higher for the STAS-negative group compared to the STAS-positive group (97.2% vs 91.4%; $P < .001$). B, The 5-year OS rate was statistically significantly higher for the STAS-negative group compared to the STAS-positive group (100% vs 94.7%; $P < .001$). For all patients in the validation cohort, the RFS rate was 96.0% and the OS rate was 97.8%. C, The 5-year RFS rate was statistically significantly higher for the STAS-negative group compared to the STAS-positive group (98.1% vs 84.8%; $P < .001$). D, The 5-year OS rate was statistically significantly higher for the STAS-negative group compared to the STAS-positive group (99.3% vs 88.7%; $P < .001$).

predicting the STAS status of clinical-stage T1N0 lung adenocarcinoma. Both methods achieved satisfactory results on the testing and external validation cohorts, indicating their capability to accurately predict the STAS status in patients with clinical-stage T1N0 lung adenocarcinoma.

Previous studies that attempted to develop models for the preoperative noninvasive detection of the CT-based STAS

status of clinical-stage T1N0 lung adenocarcinoma faced several limitations. Jiang and colleagues²⁸ predicted STAS using a random forest model, achieving an AUC of 0.75; however, the specificity of their model was relatively low at 0.59, indicating a high rate of false positives. Chen and colleagues²⁷ constructed a naïve Bayes model using 5 radiomic features to predict STAS in clinical stage I adenocarcinomas, but their AUC values were modest, at 0.63 in

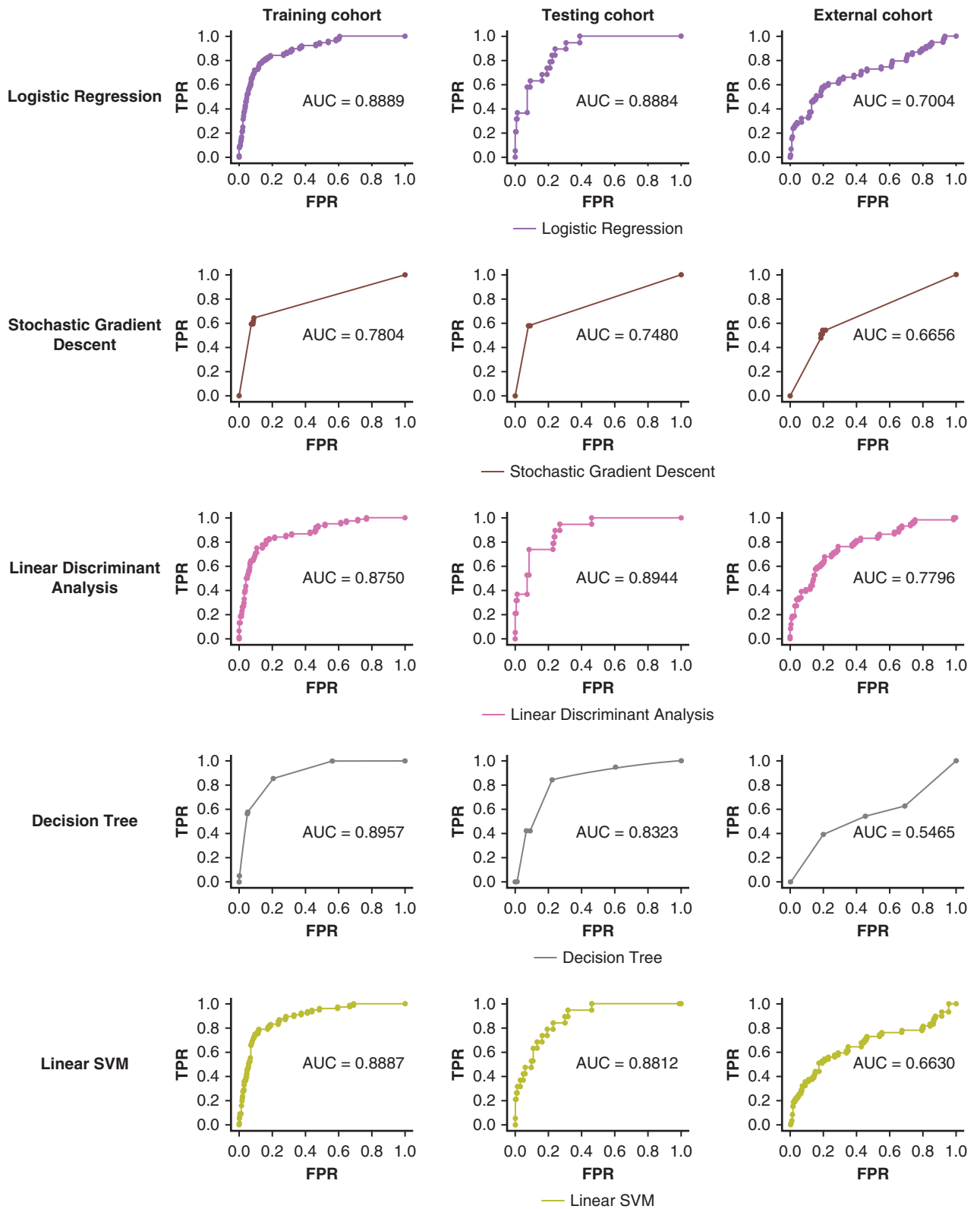
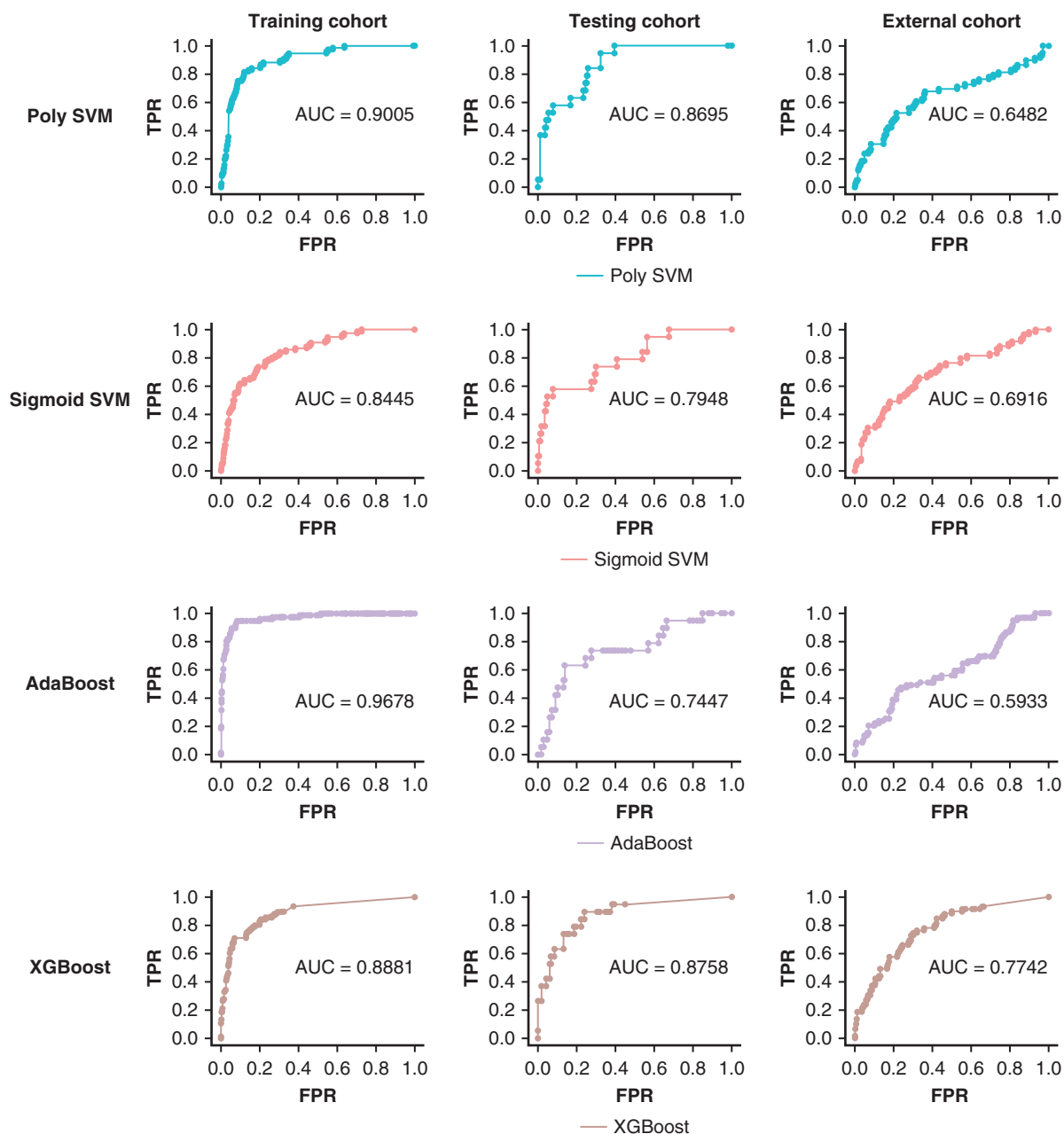


FIGURE 5. Area under the curve of (A) radiomics and (B) deep neural network DNN models for training, testing, and external validation cohorts. *TPR*, True-positive rate; *FPR*, false-positive rate.



a

FIGURE 5. (continued).

the internal validation and 0.69 in the external validation. Another prediction model²⁵ using extreme gradient boosting (XGBoost) exhibited an AUC of 0.77; however, it relied on a large number of features (n = 1874) that were extracted from a specific non-small cell lung cancer subset. Tao and colleagues²⁹ reported similar AUC values of 0.76 for their training group and 0.77 for their validation group using a traditional radiomic model, which were improved to 0.93 (95% CI, 0.70-0.82) and 0.80 (95% CI, 0.65-0.86), respectively, with a deep-learning 3D convolutional neural network model. However, that study included patients in

later stages of IB-IV (21.2%-60.5%), in whom STAS positivity is higher (24.6%-63.3%), potentially making the prediction easier.

In contrast, our present study focused on lung adenocarcinoma at an early stage (1-3 cm in size), which is notoriously difficult to predict. Our LDA radiomic model exhibited impressive AUC values of 0.8944 (95% CI, 0.8241-0.9502) in the testing cohort and 0.7796 (95% CI, 0.7089-0.8448) in the external validation cohort. Furthermore, we constructed a novel 2-stage deep-learning model, MultiCL, which achieved AUC values of 0.8434 (95% CI,

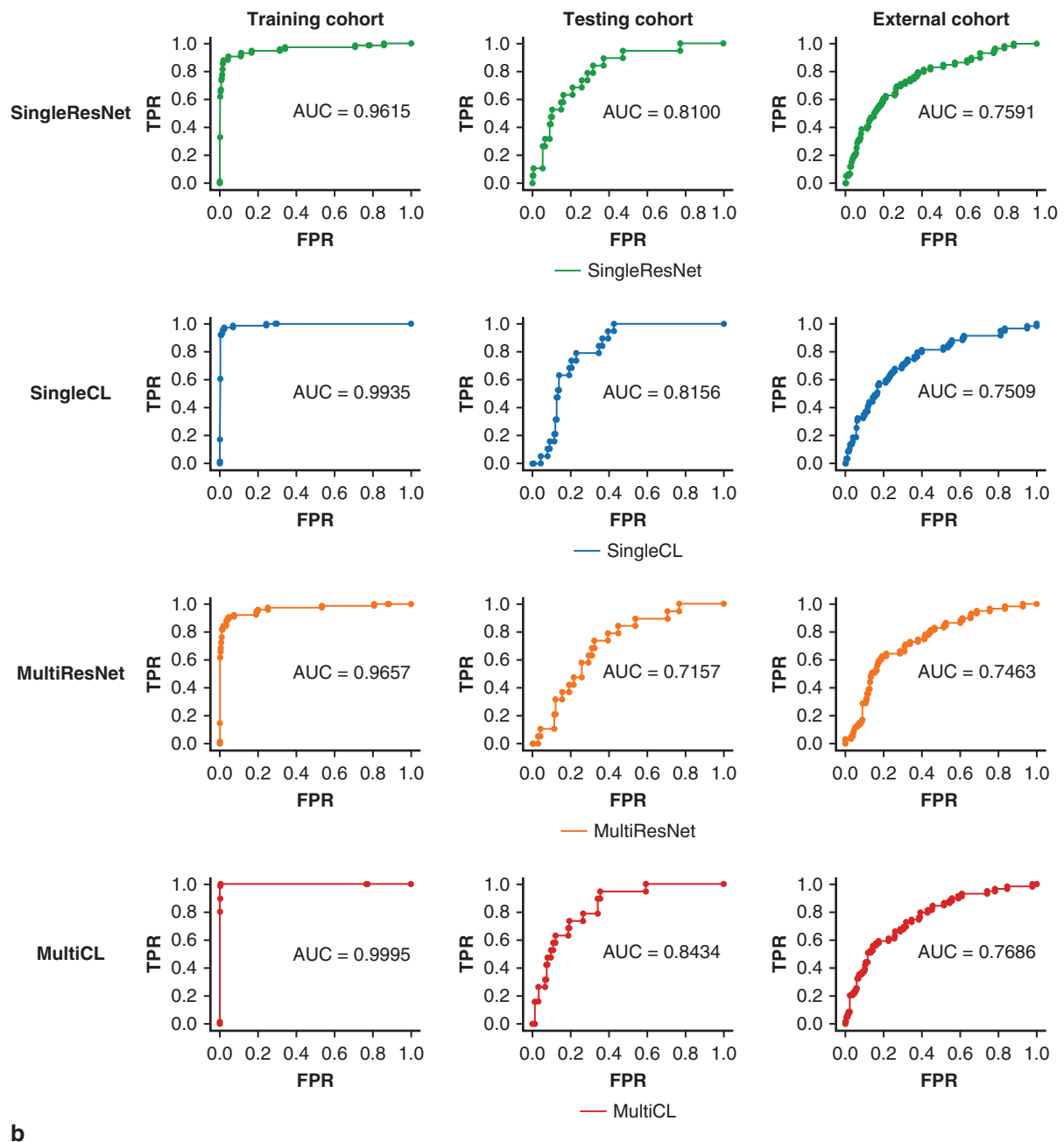


FIGURE 5. (continued).

0.7580-0.9154) in the testing cohort and 0.7686 (95% CI, 0.6991-0.8316) in the external validation cohort. These results surpass those of previous studies and exhibit remarkable stability across internal training and internal and external validation.

Clinically, our MultiCL model offers significant advantages over existing models. The decision curve analysis revealed that MultiCL confers more benefits to patients than previous models, suggesting its potential to identify STAS-positive patients most likely to benefit from

lobectomy accurately. This accuracy enhances surgical planning and reduces the risk of oncology-ineffective sublobectomy and recurrence, ultimately improving the survival rate.

In summary, our proposed models, particularly MultiCL, demonstrated superior performance in predicting the STAS status in early-stage lung adenocarcinoma compared to previous methods. This advancement serves 4 critical clinical functions: (1) precise preoperative evaluation, (2) enhanced multidisciplinary team collaboration, (3) improved patient

communication and education, and (4) support for clinical research advancements, especially in exploring biomarkers such as STAS.

This study confirms an STAS-positive incidence via postoperative pathology of approximately 10.18% (95 of 933), which appears low. This may be attributed to the fact that adenocarcinoma in situ and minimally invasive adenocarcinoma accounted for 43.62% (407 of 933) of the total study population, and no STAS was observed in this group. The STAS incidence was 18.06% (95 of 526) when focusing solely on invasive adenocarcinoma. Specifically, the incidence of STAS-positive invasive adenocarcinoma was approximately 7.60% (13 of 171) for tumor size <1 cm, 15.05% (59 of 392) for tumor size 1 to 2 cm, and 37.10% (23 of 62) for tumor size >2 to 3 cm. STAS occurrence is related to the tumor size and pathologic subtype, particularly the micropapillary or solid component. Moreover, previous studies have highlighted the importance of considering diverse clinical pathologic factors, such as solid components,³² STAS positivity,³³ and the presence of micropapillary or solid subtypes,^{34,35} all of which carry a risk of occult lymph node metastasis. In this context, the findings of JCOG studies provide valuable directions for partial lobectomy. Regarding lymph node dissection strategies, JCOG 0804⁷ suggested that only suspicious lymph nodes must be examined. In addition, JCOG 0802⁸ recommended selective lymph node dissection to reduce the risk of recurrence in patients with solid tumors. Nevertheless, our model offers a substantial basis for intraoperative lymph node dissection strategies, especially considering the risks associated with solid components, STAS positivity, and the presence of micropapillary or solid subtypes, all of which may contribute to occult lymph node metastasis.

Accurate preoperative assessment is crucial, given the complexities and risks associated with these pathologic factors. Previous studies have associated STAS positivity with relevant imaging features, such as the consolidation tumor ratio,^{36,37} positive pleural notch sign,³⁸ cystic airspaces,³⁹ solid tumors, tumor size ≥ 2 cm, and maximum standardized uptake value ≥ 2.5 .⁴⁰ These imaging features may occur in patients with tumors of 1 to 3 cm. In 1 subject in our study, the tumor was only 1 cm, but it exhibited such imaging features as solid tumor and cystic airspaces, which were pathologically confirmed as STAS. Unfortunately, the patient still experienced distant metastasis after surgery ([Online Data Supplement](#)). Given that CT signal evaluation relies mainly on the experience of radiologists, a certain degree of subjectivity exists. Different inclusion and exclusion criteria may lead to different conclusions. Therefore, a stable, reliable, and accurate preoperative CT image prediction model is needed to avoid the impact of experience disparities among the doctors reviewing the images on the manual identification results.

Whether STAS is an in vivo phenomenon or an in vitro artifact produced after cutting a tumor with a knife remains controversial.⁴¹ Some experts suggest that in such surgeries as video-assisted thoracoscopic surgery lobectomy, in which the entire resection specimen, including tumors of various size, is squeezed through a small-caliber hole in the rigid chest wall, which may lead to tumor cell detachment around the tumor.⁴² However, a recent study by Han and colleagues¹⁷ indicated that video-assisted thoracoscopic surgery was not associated with STAS. In contrast, specific biological mechanisms appear to explain this phenomenon. *ROS1* rearrangement reduces membrane E-cadherin expression in lung adenocarcinoma cells, and the loss of E-cadherin disrupts cell–cell contact, leading to tumor cell movement and STAS production.⁴³ In addition, recent studies⁴⁴ have indicated rearrangement of the *ROS1* (OR, 524.075; 95% CI, 25.622–10,719.626; $P = .000$) and *ALK* (OR, 143.104; 95% CI: 3.746–5467.253; $P = .008$) genes were rearranged, which was significantly associated with STAS. In another study,⁴⁵ 71% of patients with *ROS1* rearrangements were diagnosed with STAS. Takeuchi and colleagues⁴⁶ believed that *ALK* and *ROS1* had similar clinicopathologic features in patients with tissue and gene rearrangements. These factors may explain why *ALK* and *ROS1* gene rearrangements are significantly associated with STAS.

Tumor-driver gene mutations are typically identified postoperatively, however. Although performing preoperative blood biopsies to detect *ROS1//ALK* and then determining the surgical method is recommended in these patients, the cost of such a procedure can represent a heavy burden. Alternatively, relying on noninvasive imaging for preoperative identification may offer convenience and feasibility.

Despite its many advantages, this study has several limitations. First, this was a retrospective study, and although external validation was performed, further prospective studies are necessary for model validation. Second, our cohort comprised only patients with clinical-stage T1N0 adenocarcinoma, limiting the generalizability of our findings to other pathologic subtypes of lung cancer. The main drawback of deep-learning technology in medical imaging analysis is its black-box nature, which limits the interpretability. Addressing this opacity in future work is essential. Furthermore, there were no statistically significant differences in the RFS between STAS-positive and STAS-negative patients in our validation cohort. We believe that this is primarily attributed to the limited sample size of the validation cohort and the early stage of the disease, which prevented sufficient observation of relapsed patients, potentially obscuring statistically significant variations. Nonetheless, these limitations have minimal impact on the utility of the proposed model. The widespread use of medical imaging in clinical settings provides ample

opportunities to enhance cancer treatment decision support cost-effectively.

CONCLUSIONS

In summary, CT-based imaging models (radiomics and DNNs) offer considerable potential for predicting the STAS status in patients with clinical-stage T1N0 lung adenocarcinoma. These models can provide valuable decision support to surgeons, aiding the formulation of surgical strategies before surgery and ultimately improving patient prognosis.

Conflict of Interest Statement

The authors reported no conflicts of interest.

The *Journal* policy requires editors and reviewers to disclose conflicts of interest and to decline handling or reviewing manuscripts for which they may have a conflict of interest. The editors and reviewers of this article have no conflicts of interest.

This work was supported by the Extreme Smart Analysis platform (<https://www.xsmartanalysis.com/>).

References

- Rami-Porta R, Nishimura KK, Giroux DJ, et al. The International Association for the Study of Lung Cancer Lung Cancer Staging Project: proposals for revision of the TNM stage groups in the forthcoming (ninth) edition of the TNM classification for lung cancer. *J Thorac Oncol*. 2024;19(7):1007-1027.
- Fick CN, Dunne EG, Vanstraelen S, et al. High-risk features associated with recurrence in stage I lung adenocarcinoma. *J Thorac Cardiovasc Surg*. May 22, 2024 [Epub ahead of print].
- Wang C, Wu Y, Shao J, Liu D, Li W. Clinicopathological variables influencing overall survival, recurrence and post-recurrence survival in resected stage I non-small-cell lung cancer. *BMC Cancer*. 2020;20(1):150.
- Travis WD, Brambilla E, Nicholson AG, et al. The 2015 World Health Organization classification of lung tumors: impact of genetic, clinical and radiologic advances since the 2004 classification. *J Thorac Oncol*. 2015;10(9):1243-1260.
- Chen S, Ye T, Yang S, et al. Prognostic implication of tumor spread through air spaces in patients with pathologic N0 lung adenocarcinoma. *Lung Cancer*. 2022; 164:33-38.
- Yanagawa N, Shiono S, Endo M, Ogata SY. Tumor spread through air spaces is a useful predictor of recurrence and prognosis in stage I lung squamous cell carcinoma, but not in stage II and III. *Lung Cancer*. 2018;120:14-21.
- Suzuki K, Watanabe SI, Wakabayashi M, et al. A single-arm study of sublobar resection for ground-glass opacity dominant peripheral lung cancer. *J Thorac Cardiovasc Surg*. 2022;163(1):289-301.e2.
- Saji H, Okada M, Tsuboi M, et al. Segmentectomy versus lobectomy in small-sized peripheral non-small-cell lung cancer (JCOG0802/WJOG4607L): a multicentre, open-label, phase 3, randomised, controlled, non-inferiority trial. *Lancet*. 2022;399(10335):1607-1617.
- Aokage K, Suzuki K, Saji H, et al. Segmentectomy for ground-glass-dominant lung cancer with a tumour diameter of 3 cm or less including ground-glass opacity (JCOG1211): a multicentre, single-arm, confirmatory, phase 3 trial. *Lancet Respir Med*. 2023;11(6):540-549.
- Altorki N, Wang X, Kozono D, et al. Lobar or sublobar resection for peripheral stage IA non-small-cell lung cancer. *N Engl J Med*. 2023;388(6):489-498.
- Kadota K, Nitadori JI, Sima CS, et al. Tumor spread through air spaces is an important pattern of invasion and impacts the frequency and location of recurrences after limited resection for small stage I lung adenocarcinomas. *J Thorac Oncol*. 2015;10(5):806-814.
- Eguchi T, Kameda K, Lu S, et al. Lobectomy is associated with better outcomes than sublobar resection in spread through air spaces (STAS)-positive T1 lung adenocarcinoma: a propensity score-matched analysis. *J Thorac Oncol*. 2019; 14(1):87-98.
- Huang L, Tang L, Dai L, Shi Y. The prognostic significance of tumor spread through air space in stage I lung adenocarcinoma. *Thorac Cancer*. 2022;13(7): 997-1005.
- Li J, Wang Y, Li J, Cao S, Che G. Meta-analysis of lobectomy and sublobar resection for stage I non-small cell lung cancer with spread through air spaces. *Clin Lung Cancer*. 2022;23(3):208-213.
- Shiono S, Yanagawa N. Spread through air spaces is a predictive factor of recurrence and a prognostic factor in stage I lung adenocarcinoma. *Interact Cardiovasc Thorac Surg*. 2016;23(4):567-572.
- Dai C, Xie H, Su H, et al. Tumor spread through air spaces affects the recurrence and overall survival in patients with lung adenocarcinoma >2 to 3 cm. *J Thorac Oncol*. 2017;12(7):1052-1060.
- Han YB, Kim H, Mino-Kenudson M, et al. Tumor spread through air spaces (STAS): prognostic significance of grading in non-small cell lung cancer. *Mod Pathol*. 2021;34(3):549-561.
- Chae M, Jeon JH, Chung JH, et al. Prognostic significance of tumor spread through air spaces in patients with stage IA part-solid lung adenocarcinoma after sublobar resection. *Lung Cancer*. 2021;152:21-26.
- Ren Y, Xie H, Dai C, et al. Prognostic impact of tumor spread through air spaces in sublobar resection for IA lung adenocarcinoma patients. *Ann Surg Oncol*. 2019;26(6):1901-1908.
- Villalba JA, Shih AR, Sayo TMS, et al. Accuracy and reproducibility of intraoperative assessment on tumor spread through air spaces in stage I lung adenocarcinomas. *J Thorac Oncol*. 2021;16(4):619-629.
- Lee G, Bak SH, Lee HY. CT Radiomics in thoracic oncology: technique and clinical applications. *Nucl Med Mol Imaging*. 2018;52(2):91-98.
- Lambin P, Leijenaar RTH, Deist TM, et al. Radiomics: the bridge between medical imaging and personalized medicine. *Nat Rev Clin Oncol*. 2017;14(12): 749-762.
- Gillies RJ, Kinahan PE, Hricak H. Radiomics: images are more than pictures, they are data. *Radiology*. 2016;278(2):563-577.
- Lambin P, Rios-Velazquez E, Leijenaar R, et al. Radiomics: extracting more information from medical images using advanced feature analysis. *Eur J Cancer*. 2012;48(4):441-446.
- Onozato Y, Nakajima T, Yokota H, et al. Radiomics is feasible for prediction of spread through air spaces in patients with nonsmall cell lung cancer. *Sci Rep*. 2021;11(1):13526.
- Zhuo Y, Feng M, Yang S, et al. Radiomics nomograms of tumors and peritumoral regions for the preoperative prediction of spread through air spaces in lung adenocarcinoma. *Transl Oncol*. 2020;13(10):100820.
- Chen D, She Y, Wang T, et al. Radiomics-based prediction for tumour spread through air spaces in stage I lung adenocarcinoma using machine learning. *Eur J Cardiothorac Surg*. 2020;58(1):51-58.
- Jiang C, Luo Y, Yuan J, et al. CT-based radiomics and machine learning to predict spread through air space in lung adenocarcinoma. *Eur Radiol*. 2020;30(7): 4050-4057.
- Tao J, Liang C, Yin K, et al. 3D convolutional neural network model from contrast-enhanced CT to predict spread through air spaces in non-small cell lung cancer. *Diagn Interv Imaging*. 2022;103(11):535-544.
- Wang Y, Lyu D, Zhang D, et al. Nomogram based on clinical characteristics and radiological features for the preoperative prediction of spread through air spaces in patients with clinical stage IA non-small cell lung cancer: a multicenter study. *Diagn Interv Radiol*. 2023;29(6):771-785.
- Moreira AL, Ocampo PSS, Xia Y, et al. A grading system for invasive pulmonary adenocarcinoma: a proposal from the International Association for the Study of Lung Cancer Pathology Committee. *J Thorac Oncol*. 2020; 15(10):1599-1610.
- Seok Y, Yang HC, Kim TJ, et al. Frequency of lymph node metastasis according to the size of tumors in resected pulmonary adenocarcinoma with a size of 30 mm or smaller. *J Thorac Oncol*. 2014;9(6):818-824.
- Vaghjiani RG, Takahashi Y, Eguchi T, et al. Tumor spread through air spaces is a predictor of occult lymph node metastasis in clinical stage IA lung adenocarcinoma. *J Thorac Oncol*. 2020;15(5):792-802.
- Wang L, Jiang W, Zhan C, et al. Lymph node metastasis in clinical stage IA peripheral lung cancer. *Lung Cancer*. 2015;90(1):41-46.
- Yeh YC, Kadota K, Nitadori J, et al. International Association for the Study of Lung Cancer/American Thoracic Society/European Respiratory Society classification predicts occult lymph node metastasis in clinically mediastinal node-negative lung adenocarcinoma. *Eur J Cardiothorac Surg*. 2016;49(1):e9-e15.
- Kim SK, Kim TJ, Chung MJ, et al. Lung adenocarcinoma: CT features associated with spread through air spaces. *Radiology*. 2018;289(3):831-840.

37. De Margerie-Mellon C, Onken A, Heidinger BH, VanderLaan PA, Bankier AA. CT Manifestations of tumor spread through airspaces in pulmonary adenocarcinomas presenting as subsolid nodules. *J Thorac Imaging*. 2018;33(6):402-408.
38. Toyokawa G, Yamada Y, Tagawa T, et al. Computed tomography features of resected lung adenocarcinomas with spread through air spaces. *J Thorac Cardiovasc Surg*. 2018;156(4):1670-1676.e4.
39. Qi L, Xue K, Cai Y, Lu J, Li X, Li M. Predictors of CT morphologic features to identify spread through air spaces preoperatively in small-sized lung adenocarcinoma. *Front Oncol*. 2021;10:548430.
40. Tasnim S, Raja S, Mukhopadhyay S, et al. Preoperative predictors of spread through air spaces in lung cancer. *J Thorac Cardiovasc Surg*. November 23, 2023 [Epub ahead of print].
41. Thunnissen E, Blaauwgeers HJ, De Cuba EM, Yick CY, Flieder DB. Ex vivo artifacts and histopathologic pitfalls in the lung. *Arch Pathol Lab Med*. 2016;140(3):212-220.
42. Warth A. Spread through air spaces (STAS): a comprehensive update. *Transl Lung Cancer Res*. 2017;6(5):501-507.
43. Jin Y, Sun PL, Park SY, et al. Frequent aerogenous spread with decreased E-cadherin expression of ROS1-rearranged lung cancer predicts poor disease-free survival. *Lung Cancer*. 2015;89(3):343-349.
44. Nurmamat A, Liwei Z, Yi H, et al. Analysis of risk factors of spread through air spaces in stage IA lung adenocarcinoma. *Chin J Exp Surg*. 2022;39(11):2220-2223.
45. Lee JS, Kim EK, Kim M, Shim HS. Genetic and clinicopathologic characteristics of lung adenocarcinoma with tumor spread through air spaces. *Lung Cancer*. 2018;123:121-126.
46. Takeuchi K, Soda M, Togashi Y, et al. RET, ROS1 and ALK fusions in lung cancer. *Nat Med*. 2012;18(3):378-381.

Key Words: clinical-stage T1N0 lung adenocarcinoma, deep neural network, radiomics, spread through air spaces